



## Original Research Article

View Article Online | View Journal

## Effect of Sodium Arsenic on the Improvement of TiO<sub>2</sub>/Dye as Photosensitizers in Dye-Sensitized Solar Cells (DSSC)

Imosobomeh L. Ikhioya<sup>b,c\*</sup>, Okoye Ikechukwu Francisc<sup>a</sup><sup>a</sup>Department of Physics, Federal University Gusau, Zamfara State, Nigeria<sup>b</sup>Department of Physics and Astronomy, Faculty of Physical Sciences, University of Nigeria, Nsukka, Enugu State<sup>c</sup>National Centre for Physics, Quaid-i-Azam University Campus, Islamabad, 44000, Pakistan

## ARTICLE INFORMATION

Submitted: 04 October 2023  
 Revised: 09 November 2023  
 Accepted: 09 November 2023  
 Available online: 19 November 2023

Manuscript ID: [AJGC-2310-1451](#)Checked for Plagiarism: **Yes**

Language Editor:

[Dr. Fatimah Ramezani](#)

Editor who approved publication:

[Dr. James Bashkin](#)DOI: [10.48309/ajgc.2024.419357.1451](#)

## KEYWORDS

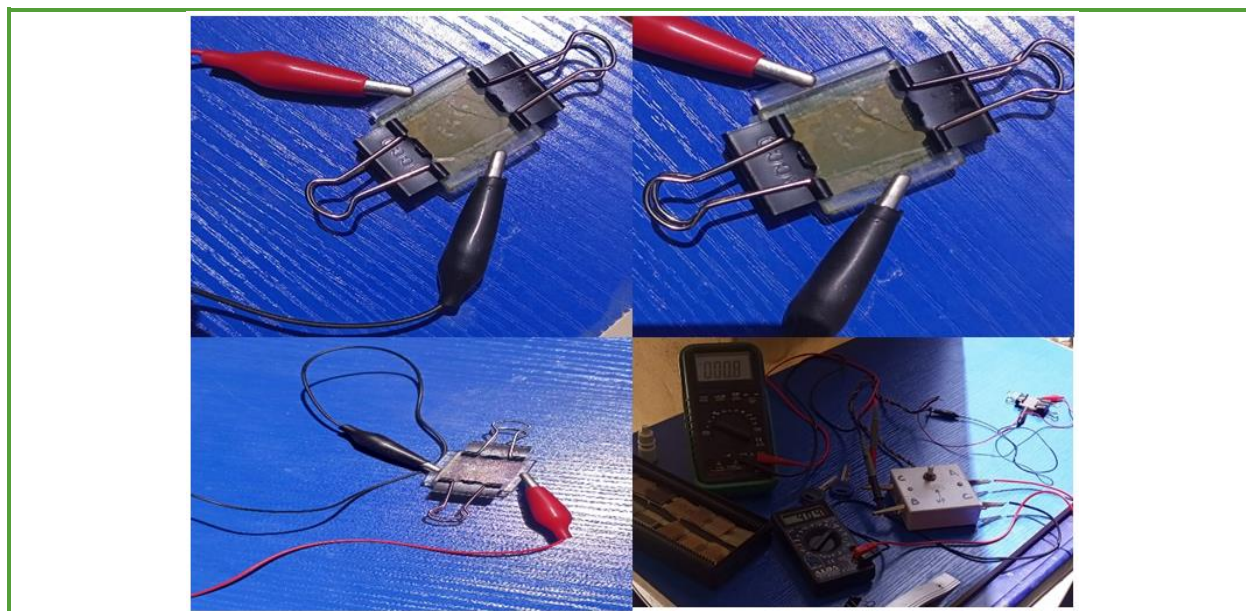
TiO<sub>2</sub>/dye  
 Solar cell  
 Grain size  
 Polycrystalline  
 Energy

## ABSTRACT

The research presents the synthesis and fabrication of dye-sensitized solar cells (DSSCs) on the influence of sodium arsenic on the enhancement of TiO<sub>2</sub>/dye as photosensitizers, where Hibiscus sabdariffa (roselle) and Vernonia amygdalina (bitter leaf) were used as a source of the chlorophyll, sodium arsenic (NaAs) material of different concentration (0.1-0.4 mol), was synthesized as a layer on top of TiO<sub>2</sub>. The surface morphology study of TiO<sub>2</sub>/NaAs<sub>0.1</sub>, TiO<sub>2</sub>/NaAs<sub>0.2</sub>/ bitter leaf dye, TiO<sub>2</sub>/NaAs<sub>0.3</sub>/ roselle dye, and TiO<sub>2</sub>/NaAs<sub>0.4</sub>/the mixture of bitter leaf dye and roselle dye revealed that the micrograph is usually defined with the granular shape of nanotubes. The grain size of TiO<sub>2</sub>/NaAs<sub>0.1</sub> is not too large and delineated by an immense sum of aggregated nanoparticles. The cells structure is polycrystalline with a most outstanding peak at 2 theta angles of 26.73° and 51.84° corresponding to hkl index numbers (111) and (202). The films have a very high absorbance from the plot, and the absorbance of the films increases as the dye molecules vary. The high absorbance of the films shows that the DSSCs will be a good material for photovoltaic applications. The fill factor of the films is 0.54, 1.24, 1.23, and 0.99 respectively while the conversion efficiency of 0.86%, 4.48%, 3.44%, and 1.81% was recorded.

© 2024 by SPC (Sami Publishing Company), Asian Journal of Green Chemistry, Reproduction is permitted for noncommercial purposes.

## Graphical Abstract



## Introduction

The world today has faced the major challenge of obtaining clean energy. Fossil fuels have been the primary energy source because they are cheap and widely accessible [1-3]. When supplies run out, it is recommended to explore and use environmentally friendly and cost-effective alternative energy sources. The sun is an eco-friendly and affordable energy source. Each hour, the sun shines on the Earth, providing more than enough energy to meet the world's energy demand for a whole year. One of several methods for converting solar energy into electrical energy is the solar cell (SC). Silicon (Si) is one of the semiconductor materials used in fabricating SCs. Si-based SC has been reported to have high efficiency ranging from 13-25%, but the major challenge limiting the use of Si as a basic material is its high cost and toxicity [4]. There are different types of solar cells, including; DSSC, organic solar cells, perovskite solar cells, and inorganic solar cells [5-7]. Among them, DSSC has outstanding properties. It provides an

economically and technically viable alternative compared to conventional solar cells. A DSSC is composed of organic dye as an absorbing layer, photoelectrode, counter electrode, and electrolyte [8]. It produces power simply by the entire lighting of organic dye in an electrochemical unit [9].

Its performance is determined by the photoelectrode component and organic dye employed. The first DSSC was initially made with a ZnO photoelectrode [10]. It had low conversion efficiency because the dye has two layers and was just able to absorb light incident on it by 1%. The DSSC performance was improved by using a porous photoelectrode, which led to the introduction of the Grätzel cell in 1991 [11], which had a 7% improved performance.

Various semiconductor materials such as gallium arsenide (GaAs), thin oxide (SnO<sub>2</sub>), indium phosphate (InP), zinc oxide (ZnO), niobium pentoxide (Nb<sub>2</sub>O<sub>5</sub>), cadmium sulfide (CdS), etc. have been employed as DSSC photoelectrode [12-14], but they show low photoconversion efficiency. Ever since 14%

efficiency was achieved in DSSC using  $\text{TiO}_2$  has been regarded as the preferred DSSC photoelectrode material [15].  $\text{TiO}_2$  has other unique features such as chemical inertness, eco-friendliness, abundance, and porosity. The wide band gap of  $\text{TiO}_2$  makes the dye molecules absorb the light spectrum over a wide range [16-18].

However, the dye molecules used in DSSCs are either natural or synthetic dyes. The natural dye (e.g., chlorophyll) obtained from flowers and plants has been employed as a DSSCs photosensitizer [19, 20]. In this research, the chlorophyll obtained from *Vernonia amygdalina* (bitter leaf) and *Hibiscus sabdariffa* (roselle) would be the dye (photosensitizer) of interest. Compared to the synthetic dye molecules, the natural dye (chlorophyll) has better advantages such as easy extraction, availability, and low cost [21, 22]. The carboxylic group found in chlorophyll increases its photoconversion efficiency [23]. Its absorption peaks range from 420-660 nm, the fill factor about 47 %, and 1.96 mA and 0.585 mV  $I_{sc}$  and  $V_{oc}$ , respectively [24]. The use of chlorophyll is limited because it can easily deteriorate when exposed to sunlight. The stability of chlorophyll is mostly improved by the formation of the complex compound via interaction with metals [25, 26]. Various mordants have been used to improve the stability of chlorophyll including; alum, chalk, metals, and salts (e.g.,  $\text{FeCl}_2$ , NaAs) [27-33]. Sodium arsenic (NaAs) is preferred and is the subject of this work. The development of complex compounds between the NaAs and chlorophyll is predicted to not only enhance heat and water resistance but also boost brightness and color retention [29]. Few researches have been carried out on improving the stability of chlorophyll using a metal mordant. This would be the first time sodium arsenic would be used to improve chlorophyll performance, stability, and coloration. H.

Darmokoesoemo *et al.* [30] studied the improved properties of the composite compound of Ni (II)-chlorophyll dye sensitizer in DSSC. Ni (II)-chlorophyll has a wide range of absorbance between the wavelengths of 295 to 665 nm. The ligand-metal bond is seen in the oscillation Ni-O at  $455.2 \text{ cm}^{-1}$  wave number. The open circuit voltage of Ni (II)-chlorophyll dye sensitizer is 0.15 V,  $I_{sc}$  is  $3.00 \text{ mAcm}^{-2}$ , and the efficiency is 0.20 %. H. Darmokoesoemo *et al.* [24] also studied the improved properties of Fe (III)-chlorophyll dye sensitizer. Classic mulberry powder (CMP) serves as the source of chlorophyll pigment. Fe (III)-chlorophyll dye sensitizer showed better performance compared to Ni (II)-chlorophyll. The Fe (III)-chlorophyll dye sensitizer has the efficiency,  $J_{sc}$  and  $V_{oc}$  of the DSSCs with Fe-chlorophyll dyes are 1.3 %,  $4 \text{ mAcm}^{-2}$ , and 0.18 V respectively. Z. Arifin *et al.* [31] studied the stability and performance of Fe-chlorophyll dye sensitizer in DSSC. The chlorophyll was obtained from papaya leaf. They reported the Fe-chlorophyll dye sensitizer to have improved stability by 2 times and efficiency by 2.5 times compared to the natural chlorophyll. The efficiency,  $J_{sc}$ , and  $V_{oc}$  of the DSSCs with Fe-chlorophyll dyes are 0.16 %,  $0.62 \text{ mAcm}^{-2}$ , and 500 mV, respectively.

Herein, we present the influence of sodium arsenic on the enhancement of dye as a photosensitizer. The chlorophyll pigments were obtained from *Vernonia amygdalina* (bitter leaf) and *Hibiscus sabdariffa* (roselle). The performance of chlorophyll photosensitizer obtained from bitter leaf, roselle, and roselle-bitter leaf combined was studied.

## Experimental

### Materials and Methods

Ethanol, sodium arsenite, and Trixon-100 were obtained from Sigma Aldrich, p25 Degussa  $\text{TiO}_2$  powder (99%), and FTO glass substrate

was obtained from the Institute of Chemical Education (ICE).

### Experimental procedure

*Hibiscus sabdariffa* (roselle) and *Vernonia amygdalina* (bitter leaf) were used as a source of chlorophyll. The leaves (samples) were weighed and crushed in a blender, and ethanol was used to dissolve the particles to harvest the chlorophyll at room temperature. The extracted dyes in the beakers were filtered using the original Whatman filter paper; the filtered chlorophyll was kept in an air-tight container to avoid degradation before use. The substrate fluorine-doped tin oxide for the fabrication of the cell (FTO) went through a series of purifications before being used.

The electrode material which is titanium dioxide ( $\text{TiO}_2$ ) was deposited using the Doctor Blade technique. The  $\text{TiO}_2$  paste was prepared using 15 ml of methanol to 6 g of  $\text{TiO}_2$  powder in a mortar with constant grinding with a pestle for proper separation of the  $\text{TiO}_2$  particles and nonionic Triton-100 was used as a surfactant to get a good paste.

The substrate was taped to get a dimension of 2.25-2.35 cm for the deposition of paste. The

samples were annealed at 350 °C for 105 mins. The Sodium arsenic (NaAs) material of different concentrations (0.1-0.4 mol) was synthesized as a layer on top of  $\text{TiO}_2$  using a spin coating machine for 5 sec. The spinning speed was 500 rpm and the films were dried in the oven for 15 minutes and the samples were taken for sanitization. The  $\text{TiO}_2$  deposited samples were buried into the extracted dyes (bitter leaf dye, roselle dye, and the mixture of bitter leaf dye and roselle dye) for 24 hours and the films were properly placed for further analysis. Graphite was used to prepare the counter electrodes on fluorine-doped tin oxide conductive glass. The extracted dyes (bitter leaf dye, roselle dye, and the mixture of bitter leaf dye and roselle dye) were analyzed for their optical, structural, and elemental studies. The electrolyte solution obtained from the Institute for Chemical Education (ICE) was dropped on the cell surface and the counter electrode with graphite was applied in contact directly with the  $\text{TiO}_2/\text{NaAs}$  substrate. The 0.2 cm strip of the film without cells was noted for the crocodile clip space by joining them together at the corner. The full cell was taken for analysis to obtain the I/V characterization (see [Figure 1](#)).

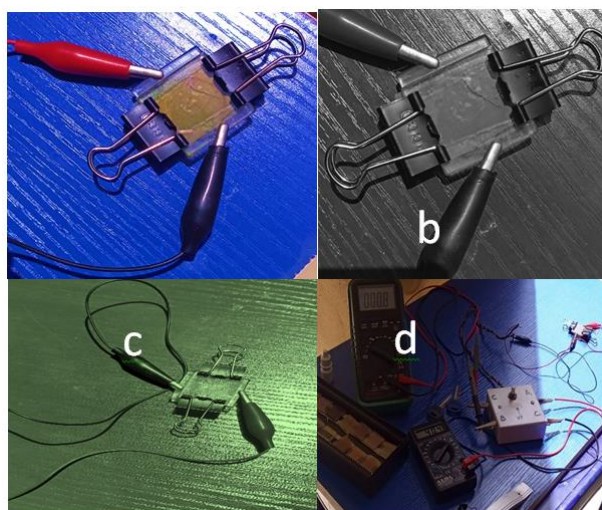


**Figure 1.** (a) Complete cell of  $\text{TiO}_2/\text{NaAs}_{0.1}$ , (b)  $\text{TiO}_2/\text{NaAs}_{0.2}$ / bitter leaf dye, (c)  $\text{TiO}_2/\text{NaAs}_{0.3}$ / roselle dye, and (d)  $\text{TiO}_2/\text{NaAs}_{0.4}$ /the mixture of bitter leaf dye and roselle dye

## Results and Discussion

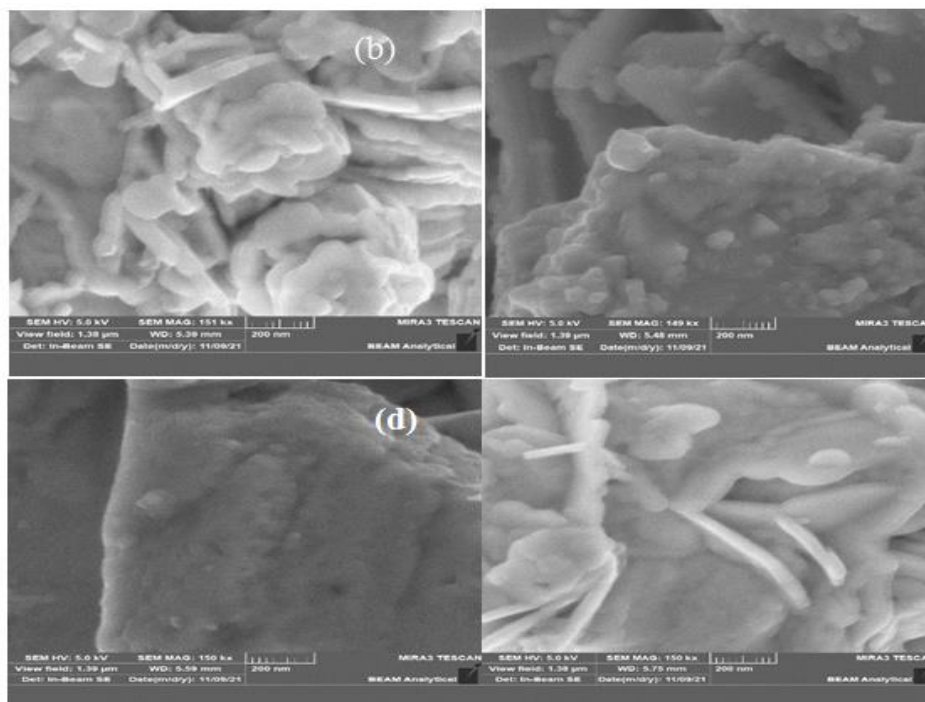
*The surface morphology study of  $TiO_2/NaAs_{0.1}$ ,  $TiO_2/NaAs_{0.2}$ / bitter leaf dye,  $TiO_2/NaAs_{0.3}$ / roselle dye, and  $TiO_2/NaAs_{0.4}$ /the mixture of bitter leaf dye and roselle dye*

Figure 2a-d demonstrates the surface morphology study of  $TiO_2/NaAs_{0.1}$ ,  $TiO_2/NaAs_{0.2}$ / bitter leaf dye,  $TiO_2/NaAs_{0.3}$ / roselle dye, and  $TiO_2/NaAs_{0.4}$ /the mixture of bitter leaf dye and roselle dye. Figure 2a illustrates that the micrograph is usually defined with the granular shape of nanotubes. The crystallite size of  $TiO_2/NaAs_{0.1}$  is not too large and delineated by an immense sum of aggregated nanoparticles  $TiO_2/NaAs_{0.2}$ / bitter leaf dye as shown in Figure 2b has smaller crystallite-sized particles of which granular shapes are more gathered. The particles clustering is evident in films synthesized with the chlorophyll of bitter leaf dye [24-31]. In Figure 2c, the distributions of the particles are random as can be seen in the non-uniformity of

the particle morphology. Moreover, firm binding power and connections with wide contact areas compel the firm bonding power of the  $TiO_2$  individual particles. The nanoparticles in Figure 2a and d suggest a better crystallite structure than the ones in Figure 5b and c.

*Elemental study of  $TiO_2/NaAs_{0.1}$ ,  $TiO_2/NaAs_{0.2}$ / bitter leaf dye,  $TiO_2/NaAs_{0.3}$ / roselle dye, and  $TiO_2/NaAs_{0.4}$ /the mixture of bitter leaf dye and roselle dye*

The spectra showing the elemental composition of  $TiO_2/NaAs_{0.1}$ ,  $TiO_2/NaAs_{0.2}$ / bitter leaf dye,  $TiO_2/NaAs_{0.3}$ / roselle dye, and  $TiO_2/NaAs_{0.4}$ /the mixture of bitter leaf dye and roselle dye is depicted in Figure 3. The spectrum shows the energy dispersive X-ray spectroscopy (EDX) of the samples. The EDX peaks show that titanium, sodium, arsenic, and oxygen are the major constituents of the particle composition, as shown in the plot.



**Figure 2.** Surface morphology of (a)  $TiO_2/NaAs_{0.1}$ , (b)  $TiO_2/NaAs_{0.2}$ / bitter leaf dye, (c)  $TiO_2/NaAs_{0.3}$ / roselle dye, and (d)  $TiO_2/NaAs_{0.4}$ /the mixture of bitter leaf dye and roselle dye

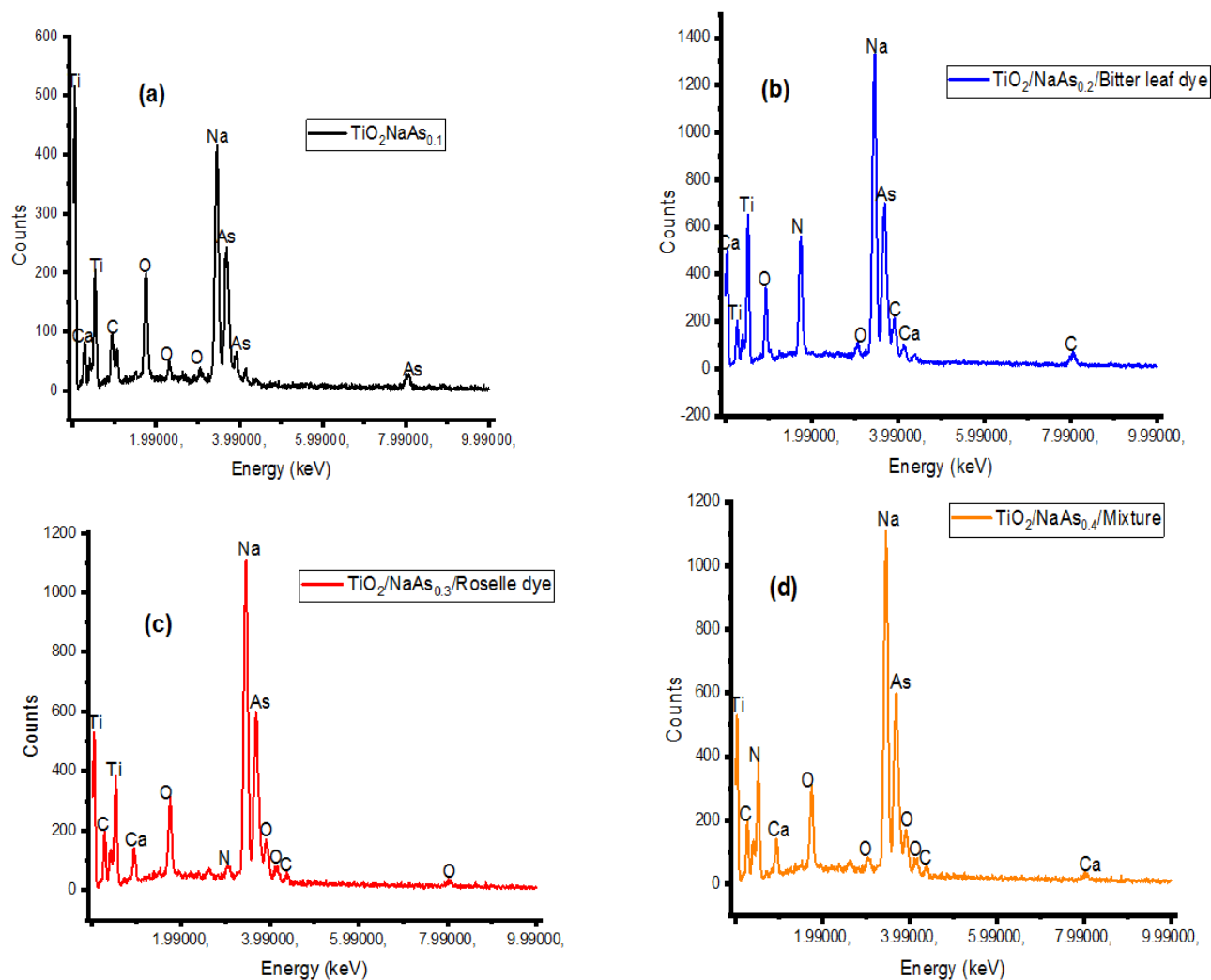


**Figure 3.** (a)  $\text{TiO}_2/\text{NaAs}_{0.1}$ , (b)  $\text{TiO}_2/\text{NaAs}_{0.2}$ / bitter leaf dye, (c)  $\text{TiO}_2/\text{NaAs}_{0.3}$ / roselle dye, and (d)  $\text{TiO}_2/\text{NaAs}_{0.4}$ /the mixture of bitter leaf dye and roselle dye

*X-ray diffraction analysis of  $\text{TiO}_2/\text{NaAs}_{0.1}$ ,  $\text{TiO}_2/\text{NaAs}_{0.2}$ / bitter leaf dye,  $\text{TiO}_2/\text{NaAs}_{0.3}$ / roselle dye, and  $\text{TiO}_2/\text{NaAs}_{0.4}$ /the mixture of bitter leaf dye and roselle dye*

The XRD study of the synthesized  $\text{TiO}_2/\text{NaAs}_{0.1}$ ,  $\text{TiO}_2/\text{NaAs}_{0.2}$ / bitter leaf dye,  $\text{TiO}_2/\text{NaAs}_{0.3}$ / roselle dye, and  $\text{TiO}_2/\text{NaAs}_{0.4}$ /the mixture of bitter leaf dye and roselle dye depicted in Figure 4 are polycrystalline with a corresponding JCPDS card number 05-4562-0976, 05-4562-0979, 05-4562-0980, and 05-4562-0988 respectively. The structure of the

cells is polycrystalline with a most outstanding peak at 2 theta angles of  $26.73^\circ$  and  $51.84^\circ$  corresponding to (111) and (202). Therefore, secondary peaks were noticed at 2 theta angles of  $37.94^\circ$  and  $65.42^\circ$  which correspond to (112) and (301), subsequently. Moreover, the diffraction peak noticed raises as the molar concentration of sodium arsenic (NaAs) increases from (0.1-0.4 mol). The rise in the intensity peak is due to the enhancement of the crystal structure and energy absorption on the lattice parameters of the  $\text{TiO}_2$ . The peak locations were not shifted due to the energy absorption of the crystals. The

structure of the lattice and single-cell distortion due to the developing increase in molar concentration of sodium arsenic (NaAs) may be concluded for the shifts in the orientation of the crystals [24-31]. The crystallite size or grain size was calculated using Equation (1).

$$D = \frac{0.9\lambda}{\beta \cos\theta} \quad (1)$$

The grain size for  $\text{TiO}_2/\text{NaAs}_{0.1}$ ,  $\text{TiO}_2/\text{NaAs}_{0.2}/$  bitter leaf dye,  $\text{TiO}_2/\text{NaAs}_{0.3}/$  roselle dye, and  $\text{TiO}_2/\text{NaAs}_{0.4}/$ the mixture of bitter leaf dye and roselle dye are presented in Table 1. It is evident that the increase in molar concentration of sodium arsenic (NaAs) increases the grain sizes and enhances the crystallinity of the films (See Table 1).

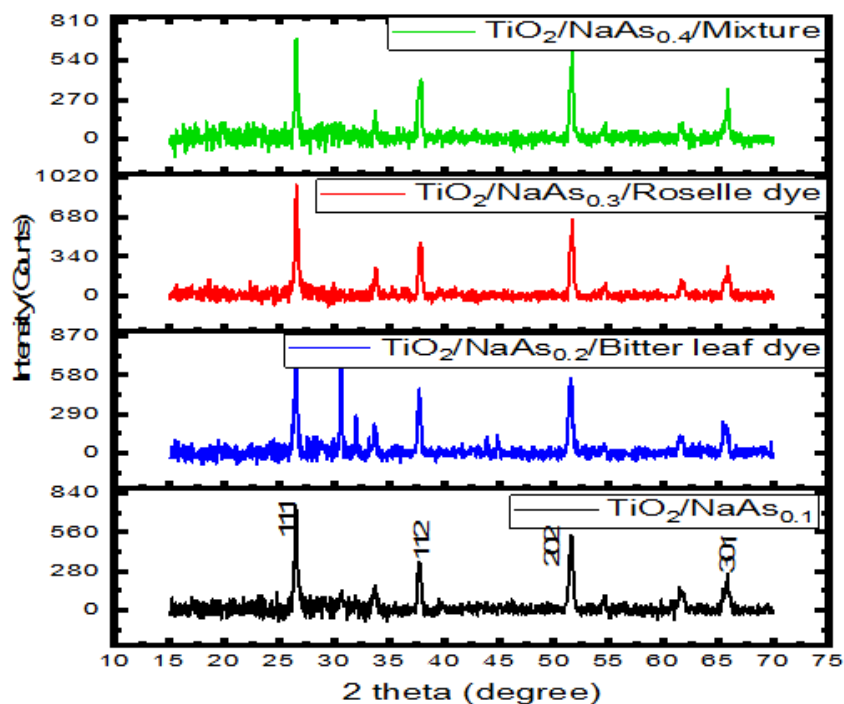


**Figure 4.** XRD spectrum of  $\text{TiO}_2/\text{NaAs}_{0.1}$ ,  $\text{TiO}_2/\text{NaAs}_{0.2}/$  bitter leaf dye,  $\text{TiO}_2/\text{NaAs}_{0.3}/$  roselle dye, and  $\text{TiO}_2/\text{NaAs}_{0.4}/$ the mixture of bitter leaf dye and roselle dye

**Table 1.** Structural parameter for  $\text{TiO}_2/\text{NaAs}_{0.1}$ ,  $\text{TiO}_2/\text{NaAs}_{0.2}/$  bitter leaf dye,  $\text{TiO}_2/\text{NaAs}_{0.3}/$  roselle dye, and  $\text{TiO}_2/\text{NaAs}_{0.4}/$ the mixture of bitter leaf dye and roselle dye

Photoanode device	$2\theta$ (Degree)	(hkl)	d- spacing (Å)	Lattice constant (a)	FWHM ( $\beta$ )	Grain Size, D (nm)	Dislocation density, $\sigma$
$\text{TiO}_2/\text{NaAs}_{0.1}$	26.73	111	3.331	5.771	0.183	0.766	5.118
$\text{TiO}_2/\text{NaAs}_{0.2}/$ Bitter leaf dye	37.94	112	2.369	4.738	0.209	0.779	6.205
$\text{TiO}_2/\text{NaAs}_{0.3}/$ Roselle dye	51.84	202	1.762	3.524	0.148	0.784	2.799
$\text{TiO}_2/\text{NaAs}_{0.4}/$ Mixture	65.42	301	1.425	3.187	0.225	0.799	5.651

*The optical study of TiO<sub>2</sub>/NaAs<sub>0.1</sub>, TiO<sub>2</sub>/NaAs<sub>0.2</sub>/ bitter leaf dye, TiO<sub>2</sub>/NaAs<sub>0.3</sub>/ roselle dye, and TiO<sub>2</sub>/NaAs<sub>0.4</sub>/the mixture of bitter leaf dye and roselle dye*

The absorbance, transmittance, and reflectance of TiO<sub>2</sub>/NaAs<sub>0.1</sub>, TiO<sub>2</sub>/NaAs<sub>0.2</sub>/ bitter leaf dye, TiO<sub>2</sub>/NaAs<sub>0.3</sub>/ roselle dye, and TiO<sub>2</sub>/NaAs<sub>0.4</sub>/the mixture of bitter leaf dye and roselle dye are displayed in Figure 5. Generally, the films have a very high absorbance from the plot, and the absorbance of the films increases as the dye molecules vary. The high absorbance of the films shows that the DSSCs will be a good material for photovoltaic applications. Figure 5 (a) presents TiO<sub>2</sub>/NaAs<sub>0.1</sub> with the lowest absorbance from the spectra and without dye molecules. It was discovered that dye molecules improve the absorbance of the films, and the *Vernonia amygdalina* (bitter leaf) dye particles have good anchoring settings on the exterior of TiO<sub>2</sub>/NaAs<sub>0.2</sub> with a better absorbance at the infrared and ultraviolet region of the spectra while *Hibiscus sabdariffa* (roselle) dye show the higher values of absorbance from the spectra at the UV region of the spectra. Both the *Vernonia amygdalina* (bitter leaf) dye molecules and *Hibiscus sabdariffa* (roselle) dye molecules give a good efficiency from the photoelectrical properties of the assembled DSSCs [24-31] which has not been reported by researchers on DSSCs. However, it clearly showed that the results obtained for TiO<sub>2</sub>/NaAs<sub>0.1</sub>, TiO<sub>2</sub>/NaAs<sub>0.2</sub>/ bitter leaf dye, TiO<sub>2</sub>/NaAs<sub>0.3</sub>/ roselle dye, and TiO<sub>2</sub>/NaAs<sub>0.4</sub>/the mixture of bitter leaf dye and roselle dye are suggested to be a good material for photovoltaic application for industrial purpose.

The transmittance of TiO<sub>2</sub>/NaAs<sub>0.1</sub>, TiO<sub>2</sub>/NaAs<sub>0.2</sub>/ bitter leaf dye, TiO<sub>2</sub>/NaAs<sub>0.3</sub>/ roselle dye, and TiO<sub>2</sub>/NaAs<sub>0.4</sub>/the mixture of bitter leaf dye and roselle dye in Figure 5b reveals a very low transmittance value due to the high absorbance of the films. A high

absorbance value usually results in low transmittance. From the spectra, it was observed that TiO<sub>2</sub>/NaAs<sub>0.1</sub> has the highest transmittance from the spectra and without dye molecules [24-31]. It was discovered that dye molecules improve the transmittance due to the high absorbance value of the films, and the *Vernonia amygdalina* (bitter leaf) dye particles have good anchoring settings on the exterior of TiO<sub>2</sub>/NaAs<sub>0.2</sub> with a better transmittance at the infrared and ultraviolet region of the spectra while *Hibiscus sabdariffa* (roselle) dye show the lower transmittance values from the spectra at both region of the spectra. Both the *Vernonia amygdalina* (bitter leaf) dye molecules and *Hibiscus sabdariffa* (roselle) dye molecules give a good efficiency from the photoelectrical properties of the assembled DSSCs which have not been reported by researchers on DSSCs.

The reflectance of TiO<sub>2</sub>/NaAs<sub>0.1</sub>, TiO<sub>2</sub>/NaAs<sub>0.2</sub>/ bitter leaf dye, TiO<sub>2</sub>/NaAs<sub>0.3</sub>/ roselle dye, and TiO<sub>2</sub>/NaAs<sub>0.4</sub>/the mixture of bitter leaf dye and roselle dye in Figure 5c revealed a negative reflectance value due to high absorbance of the films [24-31]. It is reported that dye molecules improve the absorbance of the films, and the *Vernonia amygdalina* (bitter leaf) dye particles have good anchoring settings on the exterior of TiO<sub>2</sub>/NaAs<sub>0.2</sub> with a better absorbance at the infrared and ultraviolet region of the spectra while *Hibiscus sabdariffa* (roselle) dye show the higher values of absorbance from the spectra at the UV region of the spectra, but the negative reflectance values of the films enhance the anchoring properties of the dye why perverting the films from external forces.

The energy band gap of TiO<sub>2</sub>/NaAs<sub>0.1</sub>, TiO<sub>2</sub>/NaAs<sub>0.2</sub>/ bitter leaf dye, TiO<sub>2</sub>/NaAs<sub>0.3</sub>/ roselle dye, and TiO<sub>2</sub>/NaAs<sub>0.4</sub>/the mixture of bitter leaf dye and roselle dye in Figure 6 shows that the dye has a great effect on the band gap energy of the films.

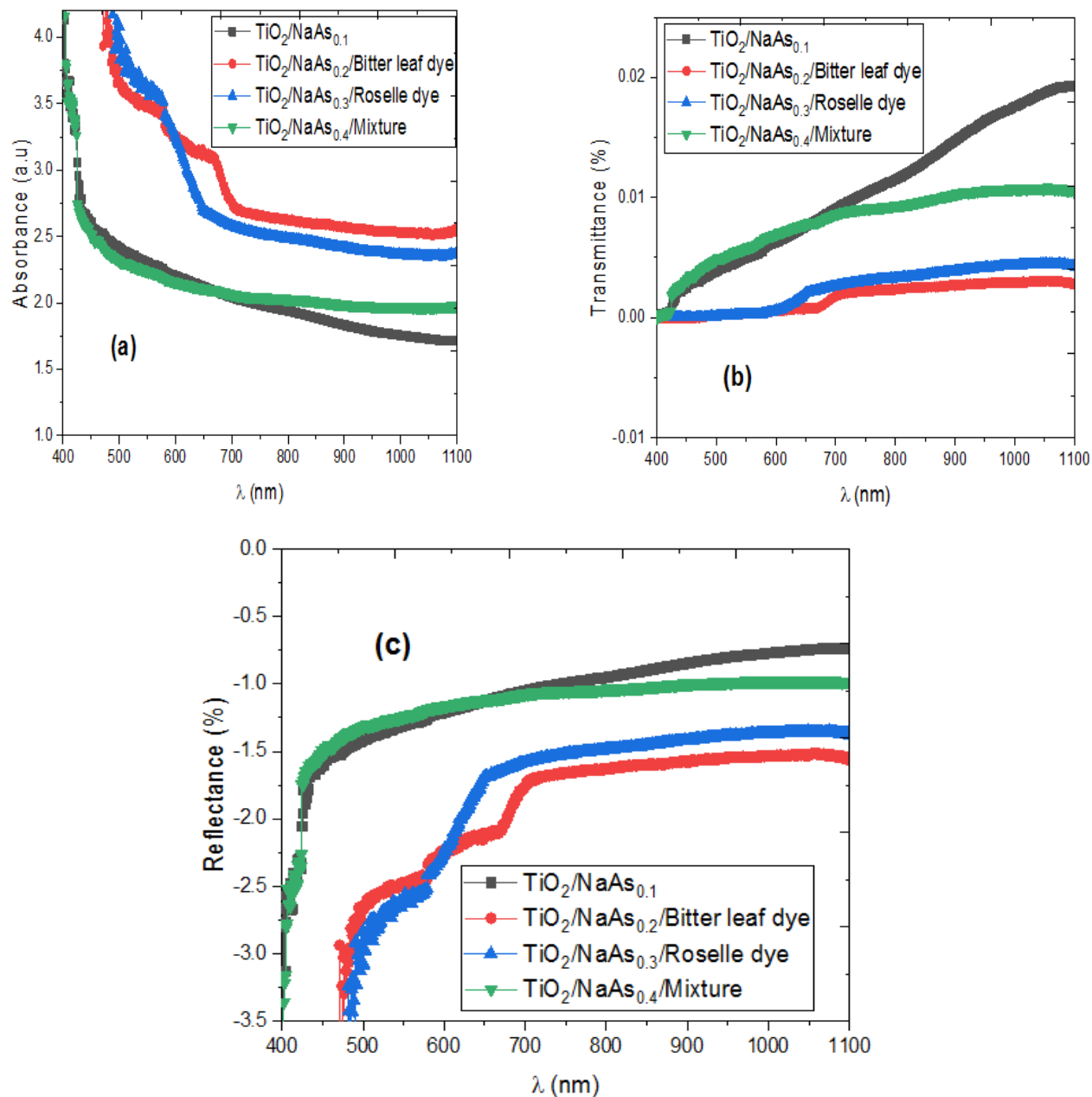


**Figure 5.** (a) absorbance, (b) transmittance, and (c) reflectance of TiO<sub>2</sub>/NaAs<sub>0.1</sub>, TiO<sub>2</sub>/NaAs<sub>0.2</sub>/ bitter leaf dye, TiO<sub>2</sub>/NaAs<sub>0.3</sub>/ roselle dye, and TiO<sub>2</sub>/NaAs<sub>0.4</sub>/the mixture of bitter leaf dye and roselle dye

The *Vernonia amygdalina* (bitter leaf) dye molecules have band gap energy of 1.70 eV which is the highest in the trend, the *Hibiscus sabdariffa* (roselle) dye molecule with an energy band gap of 1.50 eV the mixture of both dye with 1.40 eV. The plot clearly shows that the mixture of *Vernonia amygdalina* (bitter leaf) dye

and *Hibiscus sabdariffa* (roselle) dye molecules has better band gap energy [24-31].

#### Photoelectrical properties of the assembled DSSC

Table 2 summarizes the photovoltaic performance of TiO<sub>2</sub>/NaAs<sub>0.1</sub>, TiO<sub>2</sub>/NaAs<sub>0.2</sub>/ bitter leaf dye, TiO<sub>2</sub>/NaAs<sub>0.3</sub>/ roselle dye, and

TiO<sub>2</sub>/NaAs<sub>0.4</sub>/the mixture of bitter leaf dye and roselle dye of the DSSCs. The photoelectrical properties of the assembled DSSCs without natural dye and natural dye revealed that the TiO<sub>2</sub>/NaAs<sub>0.1</sub>, TiO<sub>2</sub>/NaAs<sub>0.2</sub>/ bitter leaf dye, TiO<sub>2</sub>/NaAs<sub>0.3</sub>/ roselle dye, TiO<sub>2</sub>/NaAs<sub>0.4</sub>/the mixture of bitter leaf dye, and roselle dye has J<sub>sc</sub> of 2.62 mA/cm<sup>2</sup> and V<sub>oc</sub> of 287.7 mV, J<sub>sc</sub> of 4.67 mA/cm<sup>2</sup> and V<sub>oc</sub> of 365.6 mV, J<sub>sc</sub> of 3.72 mA/cm<sup>2</sup> and V<sub>oc</sub> of 355.2 mV, and J<sub>sc</sub> of 2.92 mA/cm<sup>2</sup> and V<sub>oc</sub> of 296.7 mV, respectively. The

(FF) fill factor of TiO<sub>2</sub>/NaAs<sub>0.1</sub>, TiO<sub>2</sub>/NaAs<sub>0.2</sub>/ bitter leaf dye, TiO<sub>2</sub>/NaAs<sub>0.3</sub>/ roselle dye, and TiO<sub>2</sub>/NaAs<sub>0.4</sub>/the mixture of bitter leaf dye and roselle dye is 0.54, 1.24, 1.23, and 0.99, respectively, while the conversion efficiency of 0.86%, 4.48%, 3.44%, and 1.81% was recorded for TiO<sub>2</sub>/NaAs<sub>0.1</sub>, TiO<sub>2</sub>/NaAs<sub>0.2</sub>/ bitter leaf dye, TiO<sub>2</sub>/NaAs<sub>0.3</sub>/ roselle dye, TiO<sub>2</sub>/NaAs<sub>0.4</sub>/the mixture of bitter leaf dye, and roselle dye, subsequently.

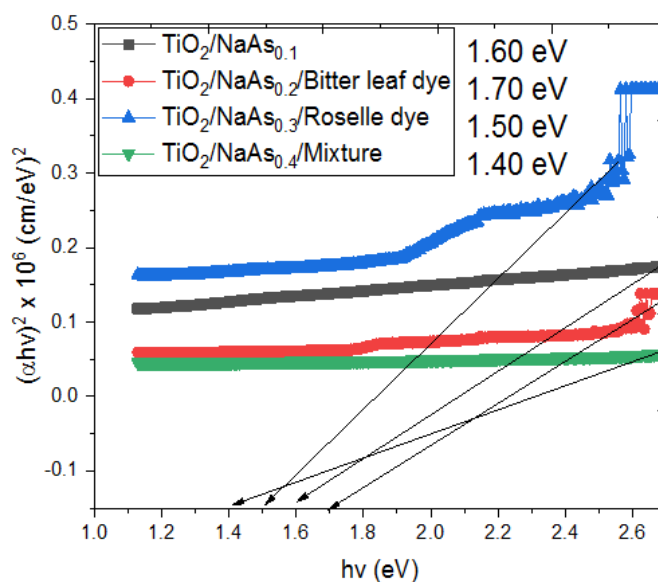


**Figure 6.** Energy band gap of TiO<sub>2</sub>/NaAs<sub>0.1</sub>, TiO<sub>2</sub>/NaAs<sub>0.2</sub>/ bitter leaf dye, TiO<sub>2</sub>/NaAs<sub>0.3</sub>/ roselle dye, and TiO<sub>2</sub>/NaAs<sub>0.4</sub>/the mixture of bitter leaf dye and roselle dye

**Table 2.** The photovoltaic performance TiO<sub>2</sub>/NaAs<sub>0.1</sub>, TiO<sub>2</sub>/NaAs<sub>0.2</sub>/ bitter leaf dye, TiO<sub>2</sub>/NaAs<sub>0.3</sub>/ roselle dye, and TiO<sub>2</sub>/NaAs<sub>0.4</sub>/the mixture of bitter leaf dye and roselle dye

Photoanode device	J <sub>sc</sub> (mAcm <sup>-2</sup> )	V <sub>oc</sub> (V)	FF	η (%)
TiO <sub>2</sub> /NaAs <sub>0.1</sub>	2.62	287.7	0.54	0.86
TiO <sub>2</sub> /NaAs <sub>0.2</sub> /Bitter leaf dye	4.67	365.6	1.24	4.48
TiO <sub>2</sub> /NaAs <sub>0.3</sub> /Roselle dye	3.72	355.2	1.23	3.44
TiO <sub>2</sub> /NaAs <sub>0.4</sub> /Mixture	2.92	296.7	0.99	1.81

The photoelectrical conversion efficiency reveals that the *Vernonia amygdalina* (bitter leaf) dye particles have better anchoring properties on the TiO<sub>2</sub>/NaAs<sub>0.2</sub> surface. Thus, the performance of TiO<sub>2</sub>/NaAs<sub>0.2</sub> DSSC is considered better when compared to the performances of

TiO<sub>2</sub>/NaAs<sub>0.3</sub> with a higher molar concentration of sodium arsenic. The facts obtained here are above the range of the results obtained by different researchers on natural dyes with the characteristic performances given in the literature [24-31].

## Conclusion

We have successfully synthesized and fabricated dye-sensitized solar cells (DSSCs) on the influence of sodium arsenic on the enhancement of TiO<sub>2</sub>/dye as photosensitizers, where Hibiscus sabdariffa (roselle) and Vernonia amygdalina (bitter leaf) were used as a source of the chlorophyll, Sodium arsenic (NaAs) material of different concentration (0.1-0.4 mol), was synthesized as a layer on top of TiO<sub>2</sub>. The surface morphology study of TiO<sub>2</sub>/NaAs<sub>0.1</sub>, TiO<sub>2</sub>/NaAs<sub>0.2</sub>/ bitter leaf dye, TiO<sub>2</sub>/NaAs<sub>0.3</sub>/ roselle dye, and TiO<sub>2</sub>/NaAs<sub>0.4</sub>/the mixture of bitter leaf dye and roselle dye revealed that the micrograph is usually defined with the granular shape of nanotubes. The grain size of TiO<sub>2</sub>/NaAs<sub>0.1</sub> is not too large and delineated by an immense sum of aggregated nanoparticles. TiO<sub>2</sub>/NaAs<sub>0.2</sub>/ bitter leaf dye as shown has smaller grain-sized particles whose shapes are granular and have more aggregated particles. The clustering of the particles is evidenced in samples synthesized with the chlorophyll of *Vernonia amygdalina* (bitter leaf). The cells structure is polycrystalline with a most outstanding peak at 2 theta angles of 26.73 ° and 51.84 ° corresponding to (111) and (202). Therefore, secondary peaks were noticed at 2 theta angles of 37.94 ° and 65.42 ° which correspond to (112) and (301) subsequently. The photoelectrical conversion efficiency reveals that the *Vernonia amygdalina* (bitter leaf) dye particles have good anchoring settings on the exterior of TiO<sub>2</sub>/NaAs<sub>0.2</sub>. Thus, the performance of TiO<sub>2</sub>/NaAs<sub>0.2</sub> DSSC is considered superior when compared to the performances of TiO<sub>2</sub>/NaAs<sub>0.3</sub> with a higher molar concentration of sodium arsenic.

## Disclosure Statement

No potential conflict of interest was reported by the authors.

## Funding

This research did not receive any specific grant from funding agencies in the public, commercial, or not-for-profit sectors.

## Authors' Contributions

All authors contributed to data analysis, drafting, and revising of the paper and agreed to be responsible for all the aspects of this work.

## References

- [1]. Cui Y., Zhao W., Ogasawara S., Wang X.-F., Tamiaki H. *J. Photochem. Photobiol. A Chem.*, 2018, **353**:625 [[Crossref](#)], [[Google Scholar](#)], [[Publisher](#)]
- [2]. Okaro C.A., Okwundu O.S., Tagbo P.C., Ugwuoke C.O., Ezugwu S., Ezema F.I. *Chemically Deposited Nanocrystalline Metal Oxide Thin Films: Synthesis, Characterizations, and Applications*. Springer, 2021, 561 [[Crossref](#)], [[Google Scholar](#)], [[Publisher](#)]
- [3]. Li G., Sheng L., Li T., Hu J., Li P., Wang K. *Sol. Energy*, 2019, **177**:80 [[Crossref](#)], [[Google Scholar](#)], [[Publisher](#)]
- [4]. Ikhioya I.L., Ugwuoke C.O., Obodo R.M., Okoli D., Eze C.U., Maaza M., Ezema F.I. *Appl. Surf. Adv.*, 2022, **9**:100232 [[Crossref](#)], [[Google Scholar](#)], [[Publisher](#)]
- [5]. Ugwuoke C.O., Ezugwu S., Mammah S., Ekwealor A., Suguyima M., Ezema F.I. *Electrode materials in energy storage and conversion*. Taylor & Francis, 2021, 321 [[Crossref](#)], [[Google Scholar](#)], [[Publisher](#)]
- [6]. Samy M., Salem M., Abdolkader T. *Int. J. Mater. Technol. Innov.*, 2021, **1**:81 [[Crossref](#)], [[Google Scholar](#)], [[Publisher](#)]
- [7]. Ijeh R.O., Ugwuoke C.O., Ugwu E.B., Aisida S.O., Ezema F.I. *Ceram. Int.*, 2022, **48**:4686 [[Crossref](#)], [[Google Scholar](#)], [[Publisher](#)]
- [8]. CUgwuoke C.O., Ezugwu S., Mammah S., Ekwealor A., Ezema F.I. *Electrode materials in*

- energy storage and conversion, 2021, 421 [Crossref], [Publisher]
- [9]. Torchani A., Saadaoui S., Gharbi R., Fathallah M. *Curr. Appl. Phys.*, 2015, **15**:307 [Crossref], [Google Scholar], [Publisher]
- [10]. Sharma K., Sharma V., Sharma S. *Nanoscale Res. Lett.*, 2018, **13**:1 [Crossref], [Google Scholar], [Publisher]
- [11]. O'regan B., Grätzel M. *Nature*, 1991, **353**:737 [Crossref], [Google Scholar], [Publisher]
- [12]. Wali Q., Bakr Z.H., Manshor N.A., Fakharuddin A., Jose R. *Sol. Energy*, 2016, **132**:395 [Crossref], [Google Scholar], [Publisher]
- [13]. Beedri N.I., Baviskar P.K., Supekar A.T., Inamuddin, Jadkar S.R., Pathan H.M. *Int. J. Mod. Phys. B*, 2018, **32**:1840046 [Crossref], [Google Scholar], [Publisher]
- [14]. Nunes B.N., Faustino L.A., Muller A.V., Polo A.S., Patrocinio A.O.T. *Nanomaterials for solar cell applications*, 2019, 287 [Crossref], [Google Scholar], [Publisher]
- [15]. Onah E.O., Offiah S., Chime U., Whyte G., Obodo R.M., Ekechukwu O., Ahmad I., Ugwuoke P., Ezema F.I. *Surfaces and Interfaces*, 2020, **20**:100619 [Crossref], [Google Scholar], [Publisher]
- [16]. Ananth S., Arumanayagam T., Vivek P., Murugakoothan P. *Optik*, 2014, **125**:495 [Crossref], [Google Scholar], [Publisher]
- [17]. Hao S., Wu J., Fan L., Huang Y., Lin J., Wei Y. *Sol. Energy*, 2004, **76**:745 [Crossref], [Google Scholar], [Publisher]
- [18]. Chou C.-S., Guo M.-G., Liu K.-H., Chen Y.-S. *Appl. Energy*, 2012, **92**:224 [Crossref], [Google Scholar], [Publisher]
- [19]. Al-Alwani M.A., Ludin N.A., Mohamad A.B., Kadhum A.A.H., Mukhlus A. *Spectrochim. Acta - Part A Mol. Biomol. Spectrosc.*, 2018, **192**:487 [Crossref], [Google Scholar], [Publisher]
- [20]. Dil M.A., Haghghatzadeh A., Mazinani B. *Bull. Mater. Sci.*, 2019, **42**:248 [Crossref], [Google Scholar], [Publisher]
- [21]. Kutraleeswarana M., Venkatachalama M., Sarojaa M., Gowthamana P., Shankara S., Parthasarathya G., Soundera J. *IAETSD J. Adv. Res. Appl. Sci.*, 2018, **5**:453
- [22]. Kim J.H., Kim D.H., So J.H., Koo H.J. *Energies*, 2021, **15**:219 [Crossref], [Google Scholar], [Publisher]
- [23]. Koyama Y., Miki T., Wang X.-F., Nagae H. *Int. J. Mol. Sci.*, 2009, **10**:4575 [Crossref], [Google Scholar], [Publisher]
- [24]. Setyawati H., Darmokoesoemo H., Ningtyas A.T.A., Kadmi Y., Elmsellem H., Kusuma H.S. *Results Phys.*, 2017, **7**:2907 [Crossref], [Google Scholar], [Publisher]
- [25]. Zhao X.Z., Jiang T., Wang L., Yang H., Zhang S., Zhou P. *J. Mol. Struct.*, 2010, **984**:316 [Crossref], [Google Scholar], [Publisher]
- [26]. Refat M.S. *Spectrochim. Acta. Part A*, 2013, **105**:326 [Crossref], [Google Scholar], [Publisher]
- [27]. Erten-Ela S., Ocakoglu K., Tarnowska A., Vakuliuk O., Gryko D.T. *Dye. Pigment*, 2015, **114**:129 [Crossref], [Google Scholar], [Publisher]
- [28]. Srinivasan V., Pavithra N., Anandan S., Jaccob M., Kathiravan A. *J. Mol. Struct.*, 2017, **1134**:112 [Crossref], [Google Scholar], [Publisher]
- [29]. Castillo-Robles J.A., Rocha-Rangel E., Ramírez-de-León J.A., Caballero-Rico F.C., Armendáriz-Mireles E.N. *J. Compos. Sci.*, 2021, **5**:288 [Crossref], [Google Scholar], [Publisher]
- [30]. Darmokoesoemo H., Fidyayanti A.R., Setyawati H., Kusuma H.S. *Korean Chem. Eng. Res.*, 2017, **55**:19 [Google Scholar], [Publisher]
- [31]. Arifin Z., Soeparman S., Widhiyanuriyawan D., Suyitno, Setyaji A.T. *J. Teknol.*, 2018, **80**:27 [Crossref]
- [32]. Kadhim M., Adail Glob M. *J. Chem. Rev.*, 2023, **5**:353 [Crossref], [Publisher]

- [33]. Agobi A.U., Louis H., Magu T.O., Dass P.M. *J. Chem. Rev*, 2019, **1**:19 [[Google Scholar](#)], [[Publisher](#)]
- [34]. Moradnia F., Fardood S.T., Ramazani A., Gupta V.K. *J. Photochem. Photobiol. A*, 2020, **392**:112433 [[Crossref](#)], [[Google Scholar](#)], [[Publisher](#)]

**How to cite this manuscript:** Okoye Ikechukwu Francis, Imosobomeh L. Ikhioya\*, Effect of Sodium Arsenic on the Improvement of TiO<sub>2</sub>/Dye as Photosensitizers in Dye-Sensitized Solar Cells (DSSC). *Asian Journal of Green Chemistry*, 8(2) 2024, 137-149.  
DOI: 10.48309/ajgc.2024.419357.1451